Jamming phase diagram for frictional particles

Massimo Pica Ciamarra,[1,*] Raffaele Pastore,[1] Mario Nicodemi,[1,2] and Antonio Coniglio[1,2]
[1]*CNR-SPIN, Dipartimento di Scienze Fisiche, Universitá di Napoli Federico II, Via Cintia, I-80126 Napoli, Italy*
[2]*INFN, Udr di Napoli, I-80126 Napoli, Italy*

(Received 8 February 2010; revised manuscript received 23 September 2011; published 28 October 2011)

We investigate the jamming transition of frictional particulate systems via discrete element simulations, reporting the existence of new regimes, which are conveniently described in a jamming phase diagram with axes density, shear stress, and friction coefficient. The resulting jammed states are characterized by different mechanical and structural properties and appear not to be "fragile" as speculated. In particular, we find a regime, characterized by extremely long processes, with a diverging time scale, whereby a suspension first flows but then suddenly jams. We link this sudden jamming transition to the presence of impeded dilatancy.

DOI: 10.1103/PhysRevE.84.041308 PACS number(s): 81.05.Rm, 64.70.ps, 83.10.Tv, 83.50.Ha

I. INTRODUCTION

The nonequilibrium transition from a fluidlike state to a disordered solidlike state, known as the jamming transition, occurs in a wide variety of many-particle systems, such as colloidal suspensions and molecular fluids, when the temperature is lowered or the density increased. Other parameters may control the transition. For instance, the applied shear stress σ has been introduced as in the "jamming phase diagram" [1–4] for particulate systems. Friction, which characterize macroscopic particles such as granular materials, is also known to influence the jamming transition [5–11]. Its role has been deeply investigated at zero applied shear stress, $\sigma = 0$, where it changes the features of the jamming that occurs on compression. Indeed, studies of frictionless systems showed that these jam at a reasonably operatively well-defined density value, the J point, identified with the random close packing volume fraction $\phi_{\rm rcp}$, and only recently demonstrated to be weakly protocol dependent [12–15]. Frictional systems, on the contrary, may jam at a volume fraction that may vary in a relatively large range [6–8,10]. In the presence of friction, the jamming density depends both on the compression protocol and on the friction coefficient. At finite shear stress, $\sigma > 0$, the jamming transition of frictional systems has been investigated to a much smaller extent but for the case of granular particles on an inclined plane, where both the normal and the shear stress change with the angle of inclination and where hysteretic effects have been reported [16]. However, there is no systematic study of the jamming transition of frictional systems in the paradigmatic constant volume and constant shear stress "ensemble" [1,2].

In this manuscript, we report a comprehensive numerical investigation of the jamming transition of frictional systems at constant volume and constant applied shear stress and show that friction controls the emergence of new dynamical regimes. Indeed, while in the absence of friction a system is either fluidlike or jammed, whereas, in the presence of friction, a system may reach a steady flowing state ("flow" regime), may jam after flowing with a constant velocity for a long time ("flow and jam" regime), may jam after a small slip ("slip and jam" regime), or may respond as a solid ("jam" regime). These features lead to the jamming phase diagram illustrated in Fig. 1, where we introduce friction as a relevant control parameter. We characterize the structural changes across the different jamming transition lines and consider the possibility that granular systems jammed at finite shear stresses display a fragile behavior [5].

The article is organized as follows. We start describing the investigated systems and the numerical procedure in Sec. II. We then illustrate in Sec. III the different dynamical regimes and show how to define their transition lines. The dependence of these lines on the friction coefficient, described in Sec. IV, leads to the jamming phase diagram. The mechanical properties of the jammed states and the concept of fragile matter are investigated in Sec. V and used to characterize the structural changes occurring across the transition lines in Sec. VI. A mechanism for the observed "flow and jam" behavior, based on the concept of impeded dilatancy, is described in Sec. VII. We draw our conclusion in Sec. VIII and describe in the appendix finite-size effects and the role of the numerical protocol.

II. MODEL SYSTEM AND NUMERICAL DETAILS

A. Investigated system

Our analysis is based on discrete element simulations of soft-core spherical grains of mass M and diameter D, enclosed between two rough plates of size $l_x = l_y = 16D$, and $l_z = 8D$, as illustrated in Fig. 2. Each plate is made by a collection of particles that move as a rigid object. The bottom plate is fix (infinite mass). The top plate has a mass equal to the sum of the masses of the constituent particles. Periodic boundary conditions are used along x and y. The system is subject to a constant shear stress, $\sigma = \sigma_{xz}$, imposed by a shear force acting on the top plate, in the absence of gravity. Periodic boundary conditions are used in the other directions.

The size of the vertical dimension l_z is chosen to be comparable to that of recent experiments [17]. We have investigated the effect of the finite size considering values of l_z to $32D$, as described in Appendix A.

B. Numerical model

We have used a standard model for the grain-grain interaction [18]. Two particles i and j, in positions $\mathbf{r}_i$ and $\mathbf{r}_j$, with linear velocities $\mathbf{v}_i$ and $\mathbf{v}_j$, and angular velocities ω_i and

*massimo.picaciamarra@spin.cnr.it

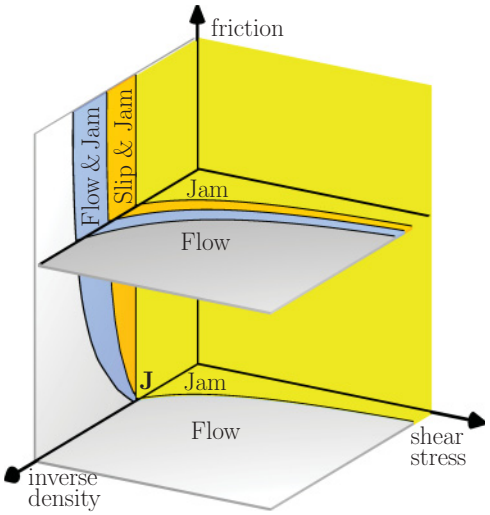

FIG. 1. (Color online) The jamming properties of frictional systems are illustrated in a diagram with axis the inverse density, the shear stress and the friction coefficient. At zero friction the jamming phase diagram is characterized by a "flow" and by a "jam" region, while in the presence of friction two new regions appear: the "flow and jam" region and the "slip and jam" region.

ω_j, interact when their separation distance $\mathbf{r}_{ij} = \mathbf{r}_i - \mathbf{r}_j$ is smaller than their diameter, i.e., when $\delta_{ij} = D - |\mathbf{r}_{ij}| \geqslant 0$. The interaction force has a normal and a tangential component.

The normal component is given by

$$\mathbf{F}_{\mathbf{n}_{ij}} = -k_n \delta_{ij} \mathbf{n}_{ij} - \gamma_n m_{\text{eff}} \mathbf{v}_{\mathbf{n}_{ij}},$$

where k_n is the elastic modulus of the particles, $\mathbf{n}_{ij} = \mathbf{r}_{ij}/|\mathbf{r}_{ij}|$, and $\mathbf{v}_{n_{ij}} = [(\mathbf{v}_i - \mathbf{v}_j) \cdot \mathbf{n}_{ij}]\mathbf{n}_{ij}$. The effective mass is $m_{\text{eff}} = M_i M_j / 2(M_i + M_j)$. The parameter γ_n is fixed in such a way that the restitution coefficient is $e = 0.88$.

The tangential component is given by

$$\mathbf{F}_{\mathbf{t}_{ij}} = -k_t \mathbf{u}_{\mathbf{t}_{ij}} - \gamma_t m_{\text{eff}} \mathbf{v}_{\mathbf{t}_{ij}},$$

where $\mathbf{u}_{\mathbf{t}_{ij}}$ is the elastic tangential displacement and $\mathbf{v}_{\mathbf{t}_{ij}} = \mathbf{v}_{ij} - \mathbf{v}_{\mathbf{n}_{ij}}$. $\mathbf{u}_{\mathbf{t}_{ij}}$, set to zero at the beginning of a contact, measures the shear displacement during the lifetime of a contact. Its time evolution is fixed by $\mathbf{v}_{\mathbf{t}_{ij}}$, ω_i, and ω_j, as described in Ref. [19]. Torques are given by $\tau_{ij} = -1/2 \mathbf{r}_{ij} \times \mathbf{F}_{t_{ij}}$. The shear

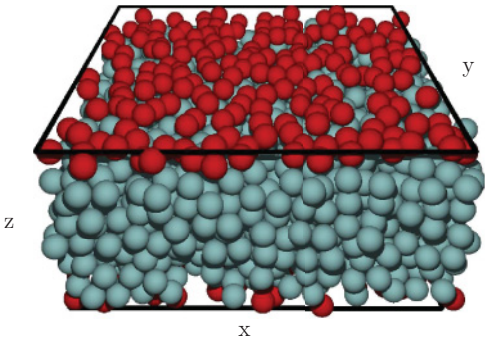

FIG. 2. (Color online) The investigated system. Grains are confined between two rough plates (red/dark particles) at a fixed vertical distance. A shear stress is fixed applying a force to the top plate; the bottom plate is fixed.

displacement is set zero at the beginning of each contact and is truncated to enforce the Coulomb condition $|\mathbf{F}_{\mathbf{t}_{ij}}| \leqslant |\mu \mathbf{F}_{\mathbf{t}_{ij}}|$ if needed. Here μ is the coefficient of static friction.

We use the value of the parameters of Ref. [19]: $k_n = 2 \times 10^5$, $k_t/k_n = 2/7$, $\gamma_n = 50$, $\gamma_t/\gamma_n = 0$. Different values of the friction coefficient are investigated. Lengths, masses, times, and stresses are measured in units of $d_0 = D$, $m_0 = M$, $t_0 = \sqrt{M/k_n}$, $\sigma_0 = k_n/D$. We solve the equations of motion of the system, $m\ddot{\mathbf{r}}_i = \sum_j \mathbf{F}_{\mathbf{n}_{ij}} + \mathbf{F}_{\mathbf{t}_{ij}}$ and $I\dot{\omega}_i = \sum_j \tau_{ij}$ via a velocity Verlet scheme, with an integration time step $\delta t = 10^{-4}$.

When the applied shear stress is $\sigma \geqslant 2 \times 10^{-3}$ (the minimum value we have considered), the system reaches its steady state after a time of the order of $T = 10^6$ time steps in all regions of the phase diagram, but for the "flow and jam" regime (see below). In this regime, simulations with $T = 5 \times 10^8$ integration time steps are needed. In $24h$, we simulate approximately a time 10^3, depending on the number of particles. We have performed simulations lasting up to 50 days. For each considered ϕ, σ, and μ point, data are averaged at least over 10 independent runs. In the "flow and jam" regime we have performed 100 runs for each considered ϕ, σ, and μ point to properly evaluate the mean jamming time.

C. Volume fraction

The volume fraction ϕ is equal to the volume occupied by the grains divided by the volume of the container. Here, we have defined the volume fraction introducing a term that takes into account the effect of the rough plates protruding into the system. Due to the boundaries, the volume accessible to the grains is not $V_0 = l_x l_y l_z$, but $V = V_0 - \Delta V$, where ΔV is an unknown corrective term. Since ΔV is much smaller than V_0, we have

$$\phi(N) = \frac{N v_0}{V_0 - \Delta V} \simeq \frac{N v_0}{V_0} \left(1 + \frac{\Delta V}{V_0}\right), \qquad (1)$$

where N is the number of enclosed grains and $v_0 = \pi/6 D^3$ is the volume occupied by a single grain. We work at constant volume and change N to set the value of the volume fraction.

We have estimated ΔV evaluating the number of grains N_{rcp} corresponding to the jamming transition, i.e., such that the generated configurations have a finite pressure for $N > N_{\text{rcp}}$. Imposing $\phi(N_{\text{rcp}}) = \phi_{\text{rcp}}$, we have determined ΔV using Eq. (1).

D. Preparation protocol

We prepare the initial state using the protocol of Ref. [10]: randomly placed small particles are grown to their final size via molecular dynamics frictionless simulations in the presence of a small viscous damping force. After inflating the particles, the system is allowed to relax until the kinetic energy vanishes. With this protocol, the jamming volume fraction at zero applied shear stress results to be $\phi_{\text{rcp}} \simeq 0.645$ [7]. Friction is introduced after these steps. Introducing friction after the inflation procedure allows for the generation of dense packings of frictional systems. Experimentally, these high-density states can be generated via more complex procedures such as vertical tapping, continuous high-frequency small amplitude vibrations [20], or thermal cycling [21]. The effect of different

preparation protocols on the reported phenomenology is described in Appendix B.

III. DYNAMICAL REGIMES

A. Overview

When the Coulomb friction coefficient μ is set to zero, our system reduces to an assembly of frictionless particlesthat either flow or respond as a solid to an applied external stress. The transition between these two regimes is assumed to occur along a well-defined jamming line, $\phi_J(\sigma)$. In making this assumption, one is considering the system large enough for finite-size effects to be negligible [3] and neglects the recently observed dependence of $\phi_J(0)$ on the protocol [12–14]. In our investigation these assumptions are reasonable, as we report a phenomenology occurring on volume fraction ranges that are greater than those of the intederminacy of $\phi_J(0)$ due to finite-size effects, and to the protocol dependence. At finite applied shear stress $\sigma > 0$, assuming the presence of a single jamming line $\phi_J(\sigma)$ means to neglect hysteretic inertial effects [22].

Our simulations at constant volume and constant shear stress show that this scenario drastically changes in the presence of friction. Indeed, we have found four different dynamical regimes, "flow," "flow and jam," "slip and jam," and "jam",[1] which are easily identified in Fig. 3, where we illustrate the time evolution of the top plate position (upper panel) and velocity (lower panel).

The behavior of the system in the different regimes can be summarized as follows. At low density, in the "flow" regime, the system flows and reaches a stationary velocity. For ϕ larger than a threshold $\phi_{J_1} = \phi_{J_1}(\sigma,\mu)$, the system enters the "flow and jam" regime. Here the system first flows with a stationary velocity (reached after a transient) but eventually enters by chance a microscopic configuration that is able to sustain the applied shear stress, and jams. The "flow and jam" region is limited by a jamming line $\phi_{J_2} = \phi_{J_2}(\sigma,\mu)$. Above ϕ_{J_2} steady flow is never observed, and the system jams after a small slip. This "slip and jam" region is limited by the line $\phi_{J_3}(\sigma,\mu)$ above which the system does not slip but responds as a solid to an applied external stress.

In this section we describe how to identify the different transition line, whose dependence on the control parameters is investigated in Sec. IV.

B. Jamming line ϕ_{J_1}

The line ϕ_{J_1} marks the transition between the "flow" and the "flow and jam" regime. In the "flow and jam" regime, the system stops flowing when a jamming configuration has been selected, after an average time $t_{\rm jam}$. We find this jamming time to grow as the volume fraction decreases, in agreement with the expectation that the lower the volume fraction, the smaller the number of configurations able to sustain the applied stress. Indeed, when the volume fraction is too small, no such configuration exists, and $t_{\rm jam}$ is infinite, as in the "flow" regime. We, therefore, define ϕ_{J_1} as the volume fraction where $t_{\rm jam}$ diverges on decreasing the volume fraction and determine it via a numerical extrapolation. Our numerical data, shown in Figs. 4(a) and 4(c) for different values of the parameters, suggest a power law divergence of the jamming time, $t_{\rm jam} \sim (\phi - \phi_{J_1})^{-\alpha}$, with α not universal.

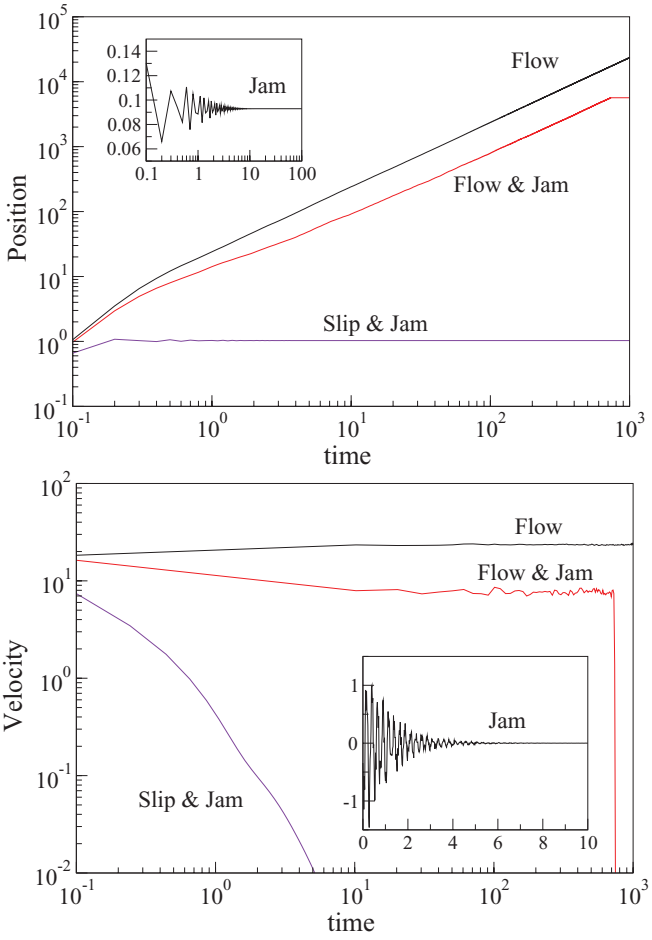

FIG. 3. (Color online) Position (upper panel) and velocity (lower panel) of the shearing top plate for $\sigma = 0.5$ and $\mu = 0.8$ and different volume fractions representative of the different flow regimes: $\phi = 0.578$ ("flow"), 0.596 ("flow and jam"), 0.629 ("slip and jam"), and 0.655 ("jam"). In the "flow" regime the system flows with a steady velocity; in the "flow and jam" regime the system first flows with a steady velocity but then jams after a time $t_{\rm jam}$; in the "slip and jam" regime the system slips of a distance ΔL, never reaching a steady velocity, and then jams. In the "jam" regime the system responds as a solid to the applied shear stress.

C. Jamming line ϕ_{J_2}

When the system reaches a steady flowing state, in the "flow" regime, it is possible to define the shear viscosity $\eta(\phi,\sigma,\mu)$ as the ratio between shear stress σ and shear rate v_s/h, where h is the distance between the two plates, and $v_s(\phi,\sigma,\mu)$ the velocity of the shearing plate. This definition is meaningful as we observe a linear velocity profile. The

[1]Another regime may be found at very high shear stresses, characterized by the ordering of the particles in planes parallel to the shearing direction [9,23–25], causing a reduction of the shear viscosity. We do not describe this ordering transition in our diagram as it occurs at shear stresses that are higher than the ones we consider.

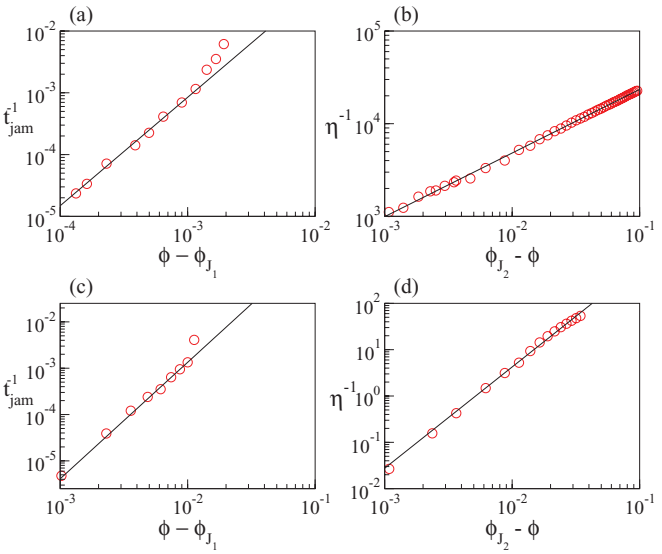

FIG. 4. (Color online) The jamming time $t_{\rm jam}$ and the viscosity η have been fitted by power laws, $t_{\rm jam} \sim (\phi - \phi_{J_1})^{-\alpha}$, $\eta \sim (\phi_{J_2} - \phi)^{-\gamma}$, for any given value of σ and μ. [(a) and (b)] Data corresponding to $\sigma = 2 \times 10^{-3}$ and $\mu = 0.1$, where $\alpha = 1.75$, $\phi_{J_1} = 0.622$, $\gamma = 0.75$, and $\phi_{J_2} = 0.625$. [(c) and (d)] The same quantities for $\sigma = 5 \times 10^{-3}$ and $\mu = 0.8$. In this case $\alpha = 2.4$, $\phi_{J_1} = 0.598$, $\gamma = 2.1$, and $\phi_{J_2} = 0.612$.

viscosity increases on increasing the volume fraction. We define ϕ_{J_2} as the volume fraction where the extrapolated viscosity diverges. We find η to diverge as a power law, $\eta \sim (\phi_{J_2} - \phi)^{-\gamma}$, with an exponent γ that appears to depend not on the shear stress but on the friction coefficient. Results for the divergence of $t_{\rm jam}$ and of η are shown in Fig. 4. We always find $\phi_{J_2} > \phi_{J_1}$, as expected, considering that the system flows with a finite shear rate at $\phi = \phi_{J_1}$.

Note that it is also possible to measure the shear viscosity in the "flow and jam" regime, as for $t < t_{\rm jam}$ the system flows in an apparently steady state. We have used values of the viscosity in this regime to reduce the error on the estimation of ϕ_{J_2}.

D. Jamming line ϕ_{J_3}

The line ϕ_{J_3} marks the end of the "slip and jam" regime, where the system slips a distance $\Delta L(\phi,\sigma)$ before jamming. We, therefore, define ϕ_{J_3} as the volume fraction where ΔL vanishes. To measure ΔL one needs to consider that the total displacement of the top plate in a jammed configuration of the "slip and jam" regime includes, in addition to the slip distance ΔL, a contribution due to the deformation induced by the shear stress. This additional deformation disappears when the shear stress is set back to zero. We have, therefore, defined the slip ΔL as the residual displacement of the top plate in a stress cycle: After preparing the system we slowly increase the stress to its final value σ and then decrease it to zero. Figure 5 (top panel) shows the displacement of the top plate position as a function of the shear stress for $\sigma = 5 \times 10^{-3}$ and $\mu = 0.8$. Different curves refer to different values of the volume fraction, as indicated. At small ϕ, the initial and final positions of the top plate do not coincide, and the residual displacement is $\Delta L > 0$, while at high ϕ we find $\Delta L \simeq 0$.

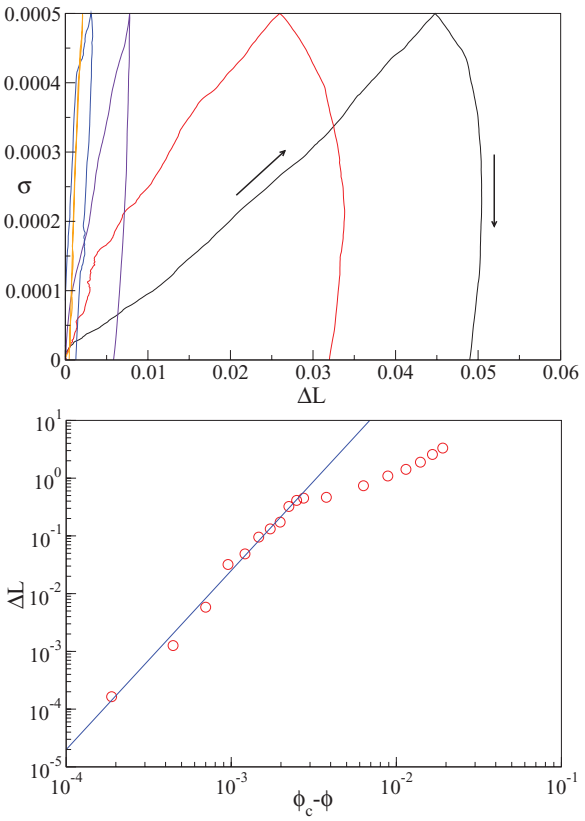

FIG. 5. (Color online) (Top) Displacement of the top plate in a stress cycle. The stress is first increased to its final value σ, and then decreased to zero. The residual displacement is our definition of the slip ΔL. From left to right, $\phi = 0.6488$, 0.6482, 0.6480, 0.6477, 0.6475. (Bottom) For a fixed value of the shear stress ($\sigma = 5 \times 10^{-3}$), the slip decreases on increasing the volume fraction, and vanishes at a volume fraction ϕ_{J_3}, which depends on σ and μ. The straight line is a power law $\Delta L = a(\phi - \phi_{J_3})^b$, $b \simeq 1.2$, and $\phi_c \simeq 0.6495$.

Precisely, when the shear stress is small, the residual displacement decreases as a power law as the volume fraction increases, which allows us to estimate ϕ_{J_3} via a numerical fit of $\Delta L(\phi)$ at each σ and μ, as illustrated in Fig. 5 (bottom panel). At high values of the shear stress, ΔL does not vanish on increasing the volume fraction, as the system deforms plastically in a stress cycle. When this is the case the dependence of ΔL on ϕ shows a clear crossover from a slip-dominated regime to a plastic-dominated regime, as shown in Fig. 6. When such a crossover is seen, we define ϕ_{J_3} as the inflection point of $\Delta L(\phi)$.

The crossover from the elastic to the plastic regime is due to the increase of the number of contacts that break as the strain increases. At small σ, the strain of the system is small, and contacts do not break. At higher σ, the strain of the system is large, and contacts break. Contact breaking appears, therefore, to be the microscopic origin of the plastic response. Indeed, memory of the tangential force between two grains is lost when the Coulomb threshold is reached.

The line ϕ_{J_3} can also be defined as that where the jamming time $t_{\rm jam}$ vanishes on increasing the density. Within numerical errors, the resulting estimate coincides with the one obtained investigating the residual slip.

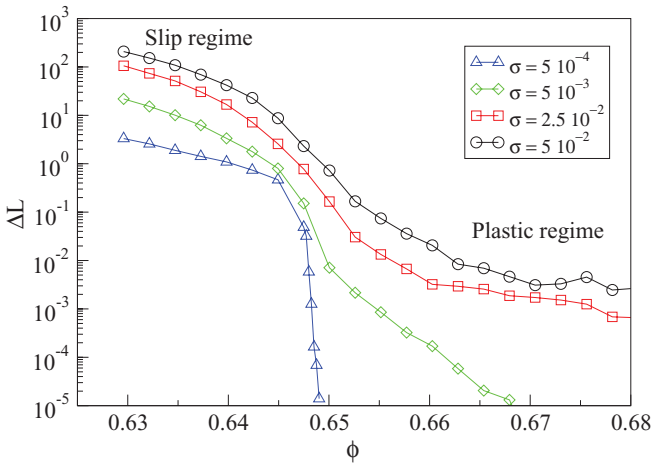

FIG. 6. (Color online) Dependence of the slip ΔL on the volume fraction ϕ, for different values of σ, at $\mu = 0.8$. When σ is small, ΔL decreases on increasing ϕ, and ϕ_{J_3} is defined as the volume fraction where ΔL vanishes, as illustrated in Fig. 5. Conversely, at high σ, ΔL does not vanish but shows a crossover from a slip-dominated regime to a plastic-dominated regime. In this case ϕ_{J_3} is defined as the inflection point of $\Delta L(\phi)$.

IV. JAMMING PHASE DIAGRAM

The location of the jamming lines depends on the model parameters. Their dependence on the applied shear stress is illustrated in Fig. 7 for two different values of the friction coefficient. As the shear stress increases, all transitions move to higher volume fractions. The dependence on the friction coefficient of ϕ_{J_1}, ϕ_{J_2}, and ϕ_{J_3} is illustrated in Fig. 8 for $\sigma = 2 \times 10^{-3}$. The dependence of ϕ_{J_3} on μ is very small and appears only at high ϕ or σ, where the system behaves plastically due to the breaking of frictional contacts. The dependence of ϕ_{J_1} and ϕ_{J_2} on μ is similar to that of different jamming thresholds found via particle inflating algorithms [7,8] or via experiments [26] and simulations [27] of sedimentation.

Extrapolating our high friction estimate of ϕ_{J_1} to the limit of zero applied shear stress, we found $\lim_{\sigma\to 0}\phi_{J_1}(\sigma) \simeq 0.585$. This estimate is close to the smallest volume fraction at which jammed states have been found via particle inflating protocols in no gravity [7]. Looser states have been found experimentally in the presence of gravity [26,28], as well as numerically in no gravity via particle deflating procedures [29]. We prefer not to link this loose density state with the random loose packing volume fraction, as this lacks an accepted theoretical definition, and is operatively defined via a different protocol (sedimentation) [26,28,30].

The dependence of the jamming lines on friction leads to the schematic jamming phase diagram for frictional particles of Fig. 1, characterized by three axis: the inverse density, the shear stress, and the friction coefficient. In this phase diagram, the surfaces $\phi_{J_1}(\sigma,\mu)$, $\phi_{J_2}(\sigma,\mu)$, and $\phi_{J_3}(\sigma,\mu)$ enclose regions of different flow properties. In this diagram, we have assumed the jamming surfaces to meet in the $\mu = 0$ plane along a well-defined jamming transition line, $\phi_J(\sigma)$, in agreement with the absence of results showing the presence of the "flow and jam" phenomenology in frictionless systems. However, as already mentioned, at zero friction neither the J point [12–14] nor the

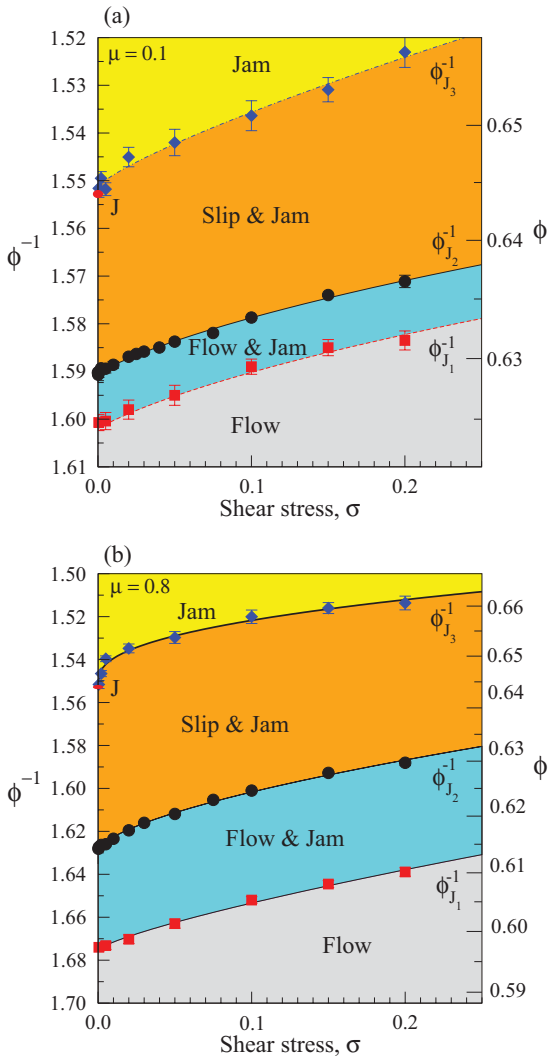

FIG. 7. (Color online) Location of the different flow regimes in the inverse density, applied stress space, for $\mu = 0.1$ (a) and $\mu = 0.8$ (b).

jamming transition line [22,31] are uniquely defined, which suggests the possible existence of an extremely small volume fraction range where the "flow and jam" and the "slip and jam" regime persist [32].

The phase diagram of Fig. 1 clarifies the intuitive expectation that when a frictional system jams after flowing, then it is possible to unjam it, not only by varying the density or the shear stress but also by changing its friction coefficient, for instance, by changing humidity or temperature or by introducing lubricants [33,34].

V. MECHANICAL RESPONSE AND FRAGILITY

Here we describe the measure of the shear modulus G. This is a quantity of interest both to characterize the jamming transitions, as well as to investigate, whereas granular jammed systems jammed at a finite value of the shear stress are fragile as speculated [5]. The concept of *fragile matter* has been introduced by M. E. Cates *et al.* [5], following earlier numerical results concerning the shear viscosity of particle suspensions

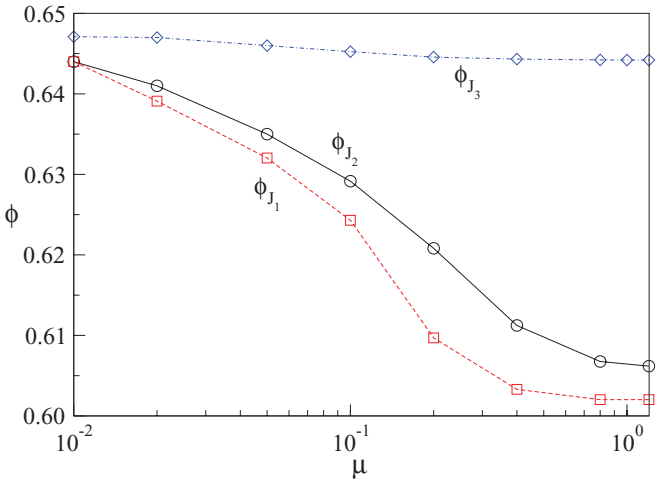

FIG. 8. (Color online) Friction dependence of the different jamming lines for $\sigma = 2 \times 10^{-3}$. Lines are a guide to the eyes.

[35], and concerns systems jammed under the action of a shear stress. In these systems, the stress is supported by an anisotropic structure. It was speculated that this anisotropy influences the mechanical properties of the system, which may depend on the relation between the perturbing stress and the pre-existing one. In particular, the system is expected to behave as a solid in response to compatible perturbations, which are those not changing the principal stress axis. Conversely, perturbations changing the principal stress axis are expected to unjam the system.

To measure the shear modulus G of a system jammed under the action of an existing shear stress σ_{xz}, we have introduced a perturbing shear stress. The nonzero components of this perturbing stress are $\delta\sigma_{xz}$ and $\delta\sigma_{yz}$, we fix in such a way that $\delta\sigma_{xz}^2 + \delta\sigma_{yz}^2 = \delta\sigma^2$. The perturbing shear stress is, therefore, conveniently expressed in terms $\delta\sigma$ and of $\theta = \arctan(\delta\sigma_{yz}/\delta\sigma_{xz})$.

Figure 9 shows the displacement $\delta\mathbf{r} = (\delta x, \delta y)$ of the top plate position for different values of ϕ at fixed σ and $\delta\sigma$

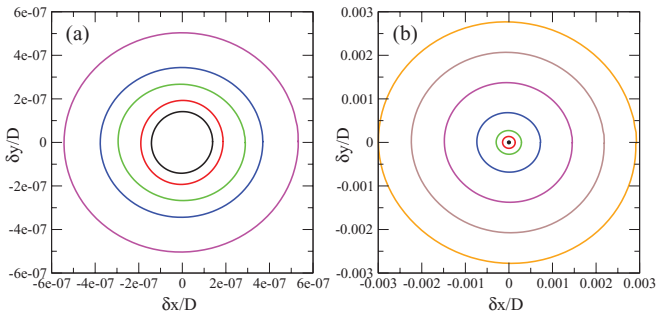

FIG. 9. (Color online) Response of a jammed system to a small perturbing shear stress. (a) The response of systems jammed under the action of a stress $\sigma = 10^{-2}$, to a perturbing stress $\delta\sigma = 10^{-4}$, for different values of the volume fraction (from the inside, ϕ =0.655, 0.630, 0.617, 0.613, and 0.610). (b) The response of system with volume fraction $\phi = 0.617$, jammed under the action of a shear stress $\sigma = 10^{-2}$, to different perturbing stresses (from the inside, $\delta\sigma = 10^{-3}, 5 \times 10^{-3}, 10^{-2}, 2.5 \times 10^{-2}, 5 \times 10^{-2}, 7.5 \times 10^{-2}, 10^{-1}$). The friction coefficient is $\mu = 0.8$.

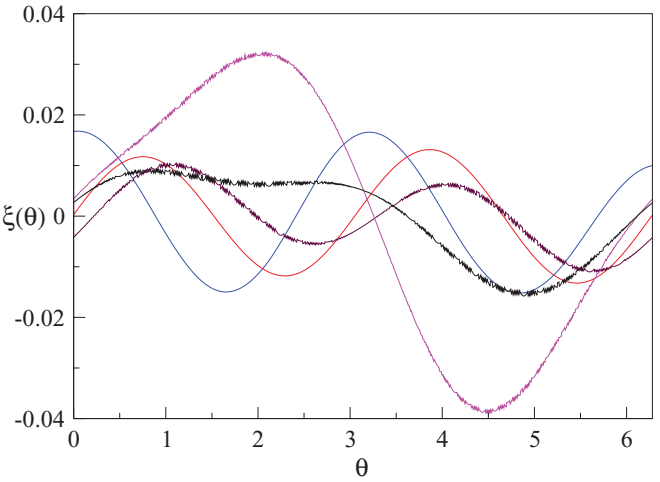

FIG. 10. (Color online) Anisotropy in the response to a small perturbing shear stress of a system jammed under the action of a large shear stress. Different curves refer to different values of the volume fraction.

(left) and for different values of $\delta\sigma$ at fixed σ and ϕ (right). Each curve is obtained by, first, applying a perturbing shear stress at $\theta = 0$ and then increasing θ from 0 to 2π. The figure clarifies that systems jammed under shear are elastic, as each curve describes a close path. Accordingly, even though their mechanical rigidity originates from an underlying force network that is highly anisotropic, these systems are not fragile as speculated [5], at least in their response to the small stress perturbations we have considered.

The absence of fragility can be rationalized in terms of the properties of the energy landscape of the system. Indeed, fragile jammed systems can be associated with saddle points, as their elastic energy may increase or decrease, depending on the direction of the perturbation, respectively, leading to an elastic response or to an instability. Since dissipative systems do not spontaneously arrest in an unstable point of their energy landscape, we expect them to arrest in a true energy minimum. Systems that jam under the action of an applied stress are, therefore, not expected to be fragile. Of course, a fragile behavior may appear in the response to large stress variations.

The curves of Fig. 9 resemble perfect circles, suggesting the presence of an isotropic response. We have verified that this is the case investigating the parameter

$$\xi(\theta) = \frac{[\delta x^2(\theta) + \delta y^2(\theta)]^{1/2} - \overline{\delta r}}{\overline{\delta r}}, \qquad (2)$$

where $\overline{\delta r} = \langle [\delta x^2(\theta) + \delta y^2(\theta)]^{1/2} \rangle_\theta$. As illustrated in Fig. 10, the anisotropy of the system is small, being $|\xi(\theta)| < 4\%$.

Due to the elastic and isotropic response of the system, we are allowed to defined the shear modulus as $G = \lim_{\delta\sigma \to 0} \delta\sigma/\epsilon$, where ϵ is the shear strain induced by $\delta\sigma$. Its behavior is described in the next section.

VI. STRUCTURAL CHANGES ACROSS THE JAMMING LINES

Here we consider how the structural properties of the system change across the jamming transitions. In particular, we focus

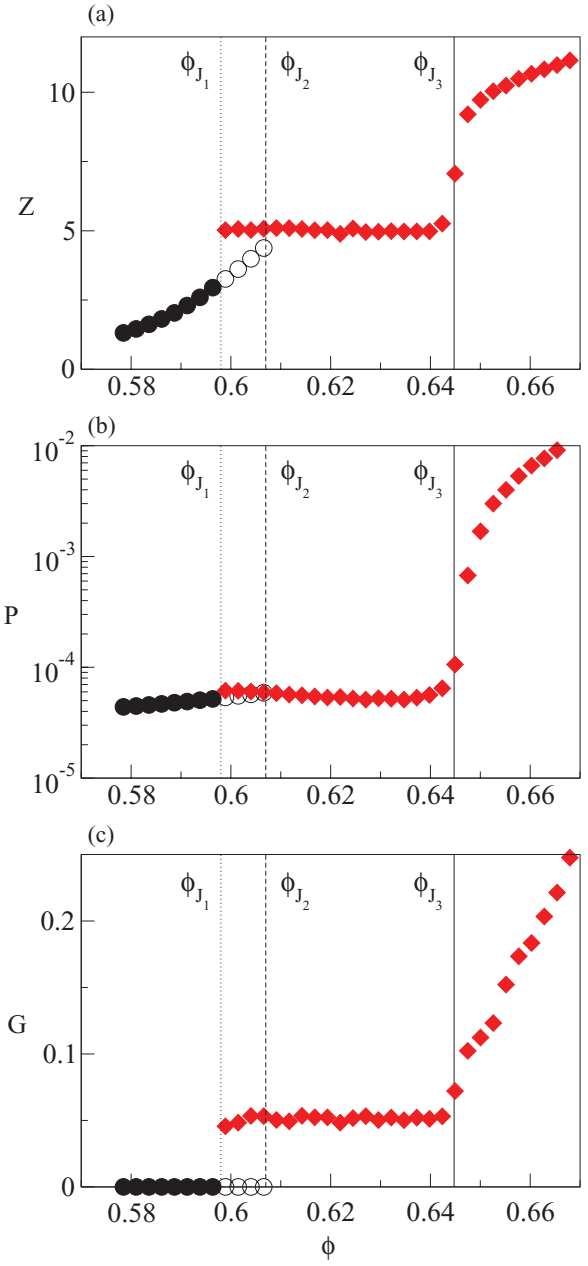

FIG. 11. (Color online) Mean contact number Z (a), normal pressure on the shearing plate P (b), and shear modulus G (c) as a function of ϕ for $\sigma = 5 \times 10^{-3}$ and $\mu = 0.8$. The vertical lines mark ϕ_{J_1}, ϕ_{J_2}, and ϕ_{J_3}, as indicated. Full circles are measures taken when the system flows, while full diamonds are measure taken in jammed configurations. Open circles in the range ϕ_{J_1}–ϕ_{J_2} are measures taken in the flowing regime for $t < t_{\rm jam}(\phi)$ before the system jams.

on the variation of the mean contact number Z, of the normal pressure on the confining walls P, and of the shear modulus G. In Fig. 11, we illustrate their volume fraction dependence for $\mu = 0.8$ and $\sigma = 5 \times 10^{-3}$. In the flowing regime (full circles) Z and P increase with ϕ, while G is zero. In the jammed regime (full diamonds) Z, P, and G are roughly constant for $\phi < \phi_{J_3}$, while they increase as power laws for $\phi > \phi_{J_3}$, where a continuous transition occurs. Measures in the flowing state in the range ϕ_{J_1}–ϕ_{J_2} (open circles) are taken for $t < t_{\rm jam}(\phi)$. Compared to previous numerical studies [7,8,11] conducted at $\sigma = 0$, our findings show that there is a whole volume fraction range where frictional granular systems may have the same mechanical properties. This volume fraction range can be identified with a constant Z line of the Z-ϕ diagram of Ref. [11].

VII. IMPEDED DILATANCY

The phenomenology observed in the "flow and jam" regime, where flowing frictional systems subject to a constant shear stress suddenly jam, may possibly be ascribed to dilatancy [36]. Dilatancy, which is the tendency of a particulate system to expand when flowing, has been mainly investigated at constant pressure, where systems can expand when flowing. At constant volume, dilatancy is impeded, and here we speculate that its effect could be the sudden jam of a flowing system.

Indeed, since dilatancy is impeded, an increase of the shear velocity may lead to an increase of the pressure, resulting both from an increase of the mean number of contacts and from an increase of the mean force between contacting grains. The increase of the confining pressure may then lead to a reduction of the shear rate and possibly to jamming. This picture is supported by the presence of a clear correlation, in the flowing regime, between the shear velocity v_s and the mean number of contacts per grain Z, whereby large values of Z occur when the shear velocity is small, as illustrated in Fig. 12. An analogous correlation is found between v_s and P, not shown. In this picture, jamming results from an impeded dilatancy induced fluctuation of the underlying network of contacts, which leads to a microscopic configuration able to support the applied shear stress. Such jammed configuration occurs when the mean number of contacts reaches a friction-dependent critical value. Note that the shear velocity fluctuations we observe at constant volume and constant shear stress can be seen as the counterpart of the anomalous pressure fluctuations found at constant volume and constant shear velocity [37–39]. However, pressure fluctuations at fixed volume and fixed shear stress are not anomalous as those observed at fixed volume and

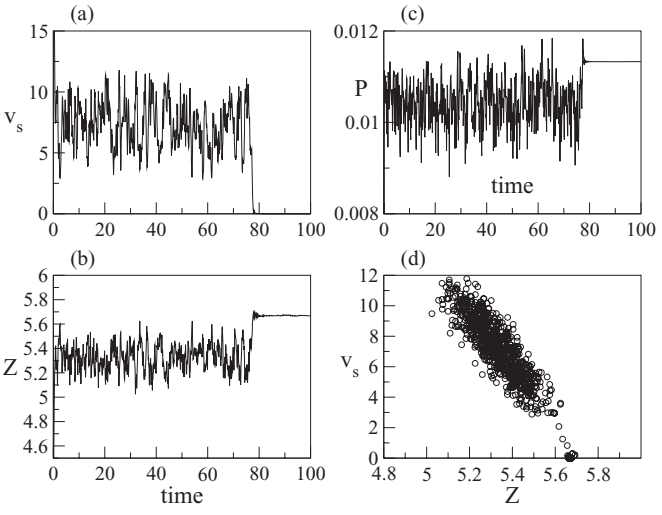

FIG. 12. Typical time dependence of the shear velocity v_s (a), of the mean contact number Z (b), and of the pressure (c) in the "flow and jam" regime. Data refer to $\mu = 0.8$, $\sigma = 1$ and $\phi = 0.606$. Panel (d) shows that Z and v_s are correlated.

fixed shear rate, as one may observe comparing, for instance, Fig. 12(c) with Fig. 1 of Ref. [37].

VIII. CONCLUSIONS

We have investigated the jamming transition of frictional particles at constant volume and constant shear stress, reporting the existence of regimes characterized by novel dynamical and structural properties. In particular, frictional granular systems may flow in an apparently steady state for a long time before they suddenly jam. While we have proposed a model to describe this dynamical jamming transition, using the concept of impeded dilatancy, a quantitative description of this transition is still lacking. In the static phase, these regimes are characterized by transitions of geometrical and mechanical quantities. In particular, when a system jams after flowing, the resulting mean contact number, pressure, and shear modulus appear to depend on the applied shear stress and not on the volume fraction. This suggests that these states could be related to the jammed states of fixed mean contact number observed at zero applied stress [11]. The study of the mechanical response of systems jammed at a finite shear stress has revealed that these systems do not exhibit a fragile behavior in response to small perturbations.

Open questions ahead include the relation of the observed jamming transitions with transitions seen at constant shear rate [40], where jamming is, by definition, precluded. In addition, the role of other parameters that are expected to control the jamming transition of frictional systems, as the confining pressure, should be also investigated. In this direction, future plans include the investigation of the role of temperature [41] in the jamming of frictional particles. Large colloidal particles, with a size of roughly 1 μm, are, in fact, at the same time small enough for temperature to influence their dynamics and large enough to be characterized by frictional forces. Indeed, dense colloidal suspensions have already shown to behave as dense granular systems [42].

ACKNOWLEDGMENTS

We gratefully acknowledge financial support from MIUR–FIRB RBFR081IUK (2008) and MIUR–PRIN 20098ZPTW7 (2009) and computer resources from the University of Naples Scope grid project, CINECA, CASPUR, and DEISA.

APPENDIX A: FINITE-SIZE EFFECTS

In this section, we discuss the robustness of the jamming phase diagram on the system size. We have performed this investigation keeping the size of the system in the transverse directions fixed, $l_x = l_y = 16D$, and varying the vertical size l_z. We compare the results for $l_z = 8$, described in the main text, with results obtained with $l_z = 16$ and $l_z = 32$. Data refer to $\sigma = 5 \times 10^{-3}$ and $\mu = 0.8$.

1. Finite-size effects at ϕ_{J_1}

The jamming volume fraction ϕ_{J_1} is that where the time $t_{\rm jam}$ a system flows in a steady state before jamming diverges on decreasing the volume fraction. The numerical identification of ϕ_{J_1} is difficult because it involves a diverging time scale, and because $t_{\rm jam}$ widely fluctuates from run to run. This implies that a large number of runs are required to reliably estimate $t_{\rm jam}$ at each value of σ, ϕ, and μ. The computational cost required to assess the presence/absence of finite-size effects at ϕ_{J_1} is, therefore, prohibitive; accordingly, while we have observed the phenomenology at all values of the system size we have considered, and also when $l_z = 64D$, we cannot exclude that this phenomenology disappears in the infinite system size limit (where it could be that $\phi_{J_1} = \phi_{J_2}$). Nevertheless, we show data clarifying that $\phi_{J_1} < \phi_{J_2}$ in very large systems, even larger than those considered in many experiments of sheared granular particles [17]. This clarifies that the reported phenomenology is experimentally relevant.

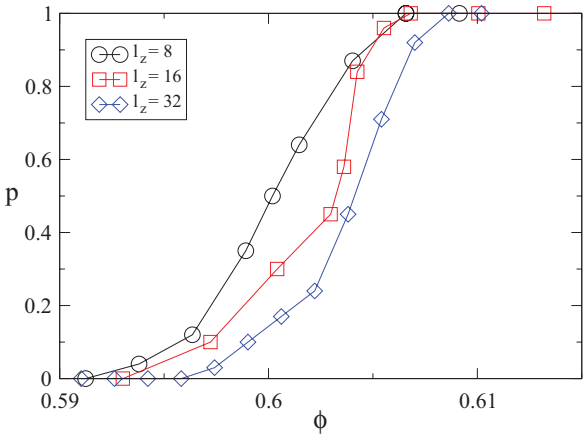

FIG. 13. (Color online) Volume fraction dependence of the fraction of simulations (over 100) jamming in a time $T = 100$ for different values of l_z.

Practically, we have determined the probability p that a simulation jams in a given time T as a function of ϕ for different values of l_z. The probability is computed over 100 runs with different initial conditions, while the simulation time is fixed to $T = 100$. The results, which are shown in Fig. 13, clarify that the "flow and jam" phenomenology is observed up

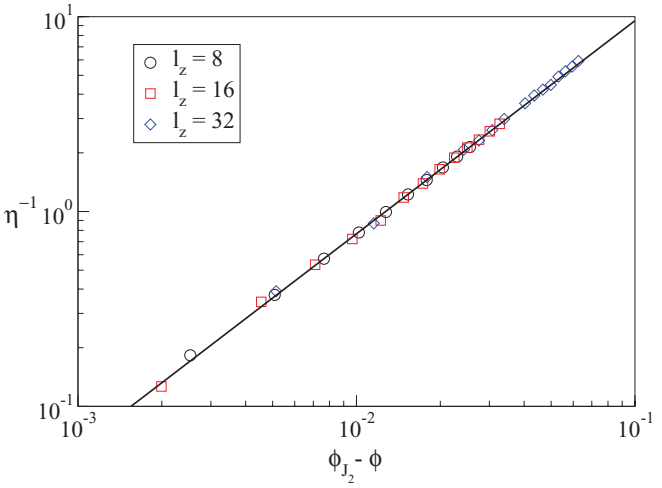

FIG. 14. (Color online) Log-log plot of the inverse shear viscosity η^{-1} versus $\phi_{J_2} - \phi$ for different system sizes. The data collapse on the same curve [$\eta^{-1} \simeq (\phi_{J_2} - \phi)^{\gamma}$, $\gamma \simeq 1.1$], indicating that finite-size effects are negligible.

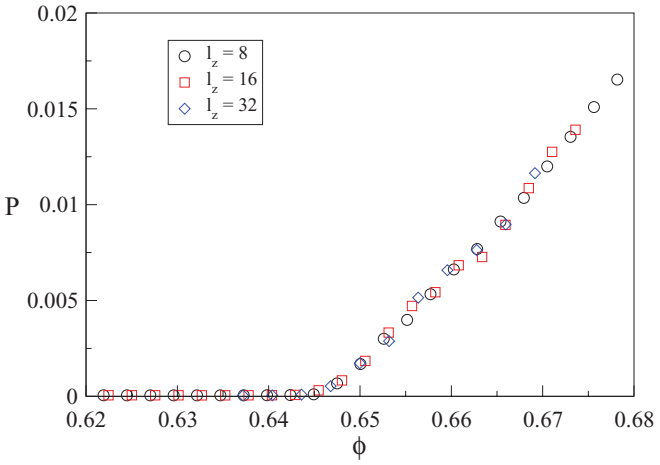

FIG. 15. (Color online) Normal pressure acting on the top confining plate as a function of the volume fraction for different system sizes.

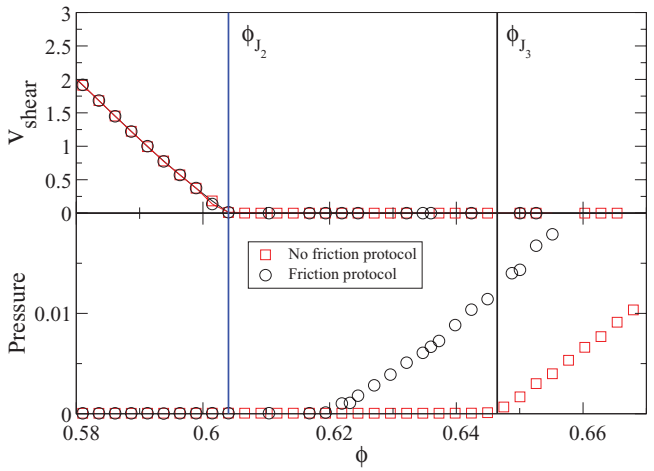

FIG. 16. (Color online) Location of the jamming transition lines as found using different protocols to prepare the initial state. ϕ_{J_1} and ϕ_{J_2} are protocol independent, while the line ϕ_{J_3} depends on the protocol. Our estimate for ϕ_{J_3} is an upper bound for all possible estimations obtained using different protocols.

to $l_z = 32$. Note that these data cannot be used to infer the fate of the ϕ_{J_1} line in the thermodynamic limit, as one should also consider the $T \to \infty$ limit.

2. Finite-size effects at ϕ_{J_2}

For each value of l_z, we have measured the shear viscosity η in the steady state, which is found to diverge as a power law at a size-independent ϕ_{J_2} value, as shown in Fig. 14. Data of different system sizes can be reasonably scaled on the same curve, which indicates that our system is large enough for finite-size effects at ϕ_{J_2} to be negligible.

3. Finite-size effects at ϕ_{J_3}

At the jamming line ϕ_{J_3}, defined as the volume fraction at which the "slip" vanishes, structural quantities have cusps, as shown in Fig. 11. To investigate the dependence of the line ϕ_{J_3} on the system size, we have studied the size dependence of the location of the cusp in the pressure. As shown in Fig. 15, the cusp occurs at the same volume fraction regardless of the system size, implying that the line ϕ_{J_3} is not affected by finite-size effects.

APPENDIX B: PREPARATION PROTOCOLS

Due to the presence of frictional forces, the response of granular systems to applied perturbations may depend on the particular protocol used to prepare the initial state. The phenomenology described so far is observed when frictional forces are introduced after the system has reached a state of zero kinetic energy at the desired volume fraction. This memoryless protocol give access to the whole zero pressure jamming phase diagram [11].

Here we consider how our findings change when the initial packing is prepared using a different and popular protocol (see, for instance, Refs. [7,43]), where friction is always taken into account. Frictional grains, initially placed in random positions with small radii, are inflated until they reach their final size. We use the same inflation rate Γ both when using the protocol considered in the manuscript ("no friction protocol"), as well as when using the modified protocol ("friction protocol"). In Fig. 16 we compare, for $\sigma = 5 \times 10^{-3}$ and $\mu = 0.8$, the velocity of the shear plate (upper panel) and the pressure (lower panel) obtained using the two protocols. The pressure is normal force acting on the top plate divided by its surface.

The shear velocity is the same regardless of the initial protocol, in agreement with the expectation that flowing systems do not remember their initial state. Accordingly, the line ϕ_{J_2}, where the viscosity diverges (the velocity vanishes), is protocol independent. The same is true for the line ϕ_{J_1} (not show), which is determined from the divergence of the jamming time, also measured when the system flows.

The pressure, which is shown in the bottom panel, has a cusp at ϕ_{J_3} (at small σ). Figure 16 clarifies that the line ϕ_{J_3} depends on the preparation protocol. The line obtained with the "no friction" protocol used in this work is an upper bound with respect to the lines obtained using other preparation protocols.

[1] A. J. Liu and S. R. Nagel, Nature **396**, 21 (1998).
[2] V. Trappe, V. Prasad, L. Cipelletti, P. N. Segre, and D. A. Weitz, Nature **411**, 772 (2001).
[3] C. S. O'Hern, L. E. Silbert, A. J. Liu, and S. R. Nagel, Phys. Rev. E **68**, 011306 (2003).
[4] A. Coniglio, A. Fierro, H. J. Herrmann, and M. Nicodemi, eds., *Unifying Concepts in Granular Media and Glasses* (Elsevier, Amsterdam, 2004).
[5] M. E. Cates, J. P. Wittmer, J. P. Bouchaud, and P. Claudin, Phys. Rev. Lett. **81**, 1841 (1998).
[6] H. A. Makse, D. L. Johnson, and L. M. Schwartz, Phys. Rev. Lett. **84**, 4160 (2000).

[7] H. P. Zhang and H. A. Makse, Phys. Rev. E **72**, 011301 (2005).
[8] K. Shundyak, M. van Hecke, and W. van Saarloos, Phys. Rev. E **75**, 010301 (2007).
[9] D. S. Grebenkov, M. P. Ciamarra, M. Nicodemi, and A. Coniglio, Phys. Rev. Lett. **100**, 078001 (2008).
[10] V. Magnanimo, L. La Ragione, J. T. Jenkins, P. Wang, and H. A. Makse, Europhys. Lett. **81**, 34006 (2008).
[11] C. Song, P. Wang, and H. A. Makse, Nature **453**, 629 (2008).
[12] M. P. Ciamarra, A. Coniglio, and A. de Candia, Soft Matter **6**, 2975 (2010).
[13] P. Chaudhuri, L. Berthier, and S. Sastry, Phys. Rev. Lett. **104**, 165701 (2010).
[14] M. Hermes and M. Dijkstra, Europhys. Lett. **89**, 38005 (2010).
[15] D. Vagberg, P. Olsson, and S. Teitel, Phys. Rev. E **83**, 031307 (2011).
[16] J. Durian, *Sands Powders, and Grains: An Introduction to the Physics of Granular Materials* (Springer, Berlin, 2000).
[17] J.-C. Tsai and J. P. Gollub, Phys. Rev. E **72**, 051304 (2005); K. E. Daniels and R. P. Behringer, Phys. Rev. Lett. **94**, 168001 (2005).
[18] P. A. Cundall and O. D. L. Strack, Geotechnique **29**, 47 (1979).
[19] L. E. Silbert *et al*., Phys. Rev. E **64**, 051302 (2001).
[20] G.-J. Gao, J. Blawzdziewicz, and C. S. O'Hern, Phys. Rev. E **80**, 061303 (2009).
[21] K. Chen *et al*., Nature **442**, 257 (2006).
[22] M. P. Ciamarra and A. Coniglio, Phys. Rev. Lett. **103**, 235701 (2009).
[23] J.-C. Tsai, G. A. Voth, and J. P. Gollub, Phys. Rev. Lett. **91**, 064301 (2003).
[24] K. E. Daniels and R. P. Behringer, Phys. Rev. Lett. **94**, 168001 (2005).
[25] M. P. Ciamarra, A. Coniglio, D. De Martino, and M. Nicodemi, Eur. Phys. J. E **24**, 411 (2007).
[26] G. R. Farrell, K. M. Martini, and N. Menon, Soft Matter **6**, 2925 (2010).
[27] L. E. Silbert, D. Ertas, G. S. Grest, T. C. Halsey, and D. Levine, Phys. Rev. E **65**, 031304 (2002).
[28] G. Y. Onoda and E. G. Liniger, Phys. Rev. Lett. **64**, 2727 (1990).
[29] L. E. Silbert, Soft Matter **6**, 2918 (2010).
[30] M. P. Ciamarra and A. Coniglio, Phys. Rev. Lett. **101**, 128001 (2008).
[31] C. Heussinger and J.-L. Barrat, Phys. Rev. Lett. **102**, 218303 (2009).
[32] M. P. Ciamarra, M. Nicodemi, and A. Coniglio, Soft Matter **6**, 2871 (2010).
[33] H. Yoshizawa, Y.-L. Chen, and J. Israelachvili, J. Phys. Chem. **97**, 4128 (1993).
[34] J. Crassous, L. Bocquet, S. Ciliberto, and C. Laroche, Europhys. Lett. **47**, 562 (1999).
[35] R. S. Farr, J. R. Melrose, and R. C. Ball, Phys. Rev. E **55**, 7203 (1997); R. C. Ball and J. R. Melrose, Adv. Colloid Interface Sci. **59**, 19 (1995); J. R. Melrose and R. C. Ball, Europhys. Lett. **32**, 535 (1995).
[36] P. Reynolds, Proc. R. Inst. **2**, 354 (1886).
[37] B. Miller, C. O'Hern, and R. P. Behringer, Phys. Rev. Lett. **77**, 3110 (1996).
[38] D. Howell, R. P. Behringer, and C. Veje, Phys. Rev. Lett. **82**, 5241 (1999).
[39] R. R. Hartley and R. P. Behringer, Nature **421**, 928 (2003).
[40] M. Otsuki and H. Hayakawa, Phys. Rev. E **83**, 051301 (2011).
[41] Z. Zhang *et al*., Nature **459**, 230 (2009).
[42] P. Ballesta, R. Besseling, L. Isa, G. Petekidis, and W. C. K. Poon, Phys. Rev. Lett. **101**, 258301 (2008).
[43] E. Somfai, M. van Hecke, W. G. Ellenbroek, K. Shundyak, and W. van Saarloos, Phys. Rev. E **75**, 020301(R) (2007).